V International Conference on Computational Methods in Marine Engineering
MARINE 2013
B. Brinkmann and P. Wriggers (Eds)

ZIG-ZAG MANEUVER SIMULATION BY CFD FOR A TANKER LIKE VESSEL

G. DUBBIOSO*, D. DURANTE*, AND R. BROGLIA*

*CNR-INSEAN, the Italian Ship Model Basin, via di Vallerano 128, Rome, Italy
e-mail: giudubbioso@libero.it, danilo.durante@cnr.it, e-mail: riccardo.broglia@cnr.it

Key words: Zig-Zag maneuver, Tanker vessel, Yaw checking ability, Propeller modeling, Dynamic Overset Grids

Abstract. The zig-zag maneuver of a tanker like vessel has been simulated by means of the globally second order accurate finite volume solver χnavis. The aim is to stress the capability of the solver in predicting the yaw checking ability of a ship model characterized by a poor directional stability, an aspect that is usually exploited when performing zig-zag maneuvering. Numerical results have been compared to free running model tests. The effect of rudder rate and propeller modeling have been also investigated. The latter topic is crucial in order to draw the potentialities and further improvements of a simplified and computationally efficient propeller models.

1 INTRODUCTION

In this work the maneuvering behavior of the tanker like vessel recently considered in previous works [1, 2, 3] has been further exploited by means of the general purpose Computational Fluid Dynamic (CFD) solver χnavis. The interest on this non-standard test case is supported by the fact that the original version of this model, i.e. twin screw with a single rudder, experienced a marked unstable behavior that was impossible to predict by means of neither system based mathematical models nor the most popular hydrodynamic coefficients regressions [4]. Moreover, the comparison with the modified (and established) version, characterized by a twin rudder control system plus a central skeg, may provide a valuable insight in the effect of stern appendages and control system configuration on the dynamic response of the vessel. On these basis, this model is therefore attractive, and, at the same time, extremely challenging for the verification and validation of the capabilities of a CFD solver for predicting ship control and maneuvering qualities. Previous research was centred on the prediction of the turning circle maneuver at higher rudder angle ($\delta = 35°$). For both configurations, numerical results were in good agreement with respect to experiments, and their relative differences in terms of dynamic quality response during the transient and the stabilized phase of the maneuver were correctly

reproduced. Moreover, the use of a novel approach for modeling the presence of the propeller let it possible to emphasize the effect of propeller in-plane loads (side forces) on the dynamic response of the vessel and a closer description of rudder-propeller interaction (in case of the twin rudder configuration).

In the present work the $10° - 10°$ zig-zag maneuver of the twin rudder configuration has been numerically simulated, in order to further verify and validate the capabilities of the CFD solver in predicting a fully unsteady maneuver; this kind of maneuver is more challenging with respect to the turning circle one, because, in addition to the correct distribution of the hydrodynamic forces and moment on the hull, their time rate variation is also crucial for a correct estimation of the dynamic response. A further issue that should be further enlightened is concerned with the validity of the hybrid propeller model presented in [1] for simulating transient maneuvers; as will be described in the following, the propeller loads are computed in the framework of quasi-steady theory and, consequently, unsteady phenomena (lead-lag of self-induced velocity field or added mass) typical of a rotor functioning within a time-varying inflow have been neglected.

In this preliminary research the modeling aspects related to propeller side force and propeller loading have been addressed. Moreover, the effect of changing the rudder rotational rate has been further considered. Numerical results are compared to the experiments [12, 13] carried out at the CNR-INSEAN outdoor maneuvering basin in terms the typical yaw checking parameters (overshoot angles and overshoot times).

2 NUMERICAL METHOD

The numerical solution of the governing equations is computed by means of the solver $\chi navis$, which is a general purpose simulation code developed at CNR-INSEAN; the code yields the numerical solution of the unsteady Reynolds averaged Navier Stokes equations for Unsteady High Reynolds Number (turbulent) free surface flows around complex geometries. The main features of the numerical algorithm are briefly summarized for the sake of brevity; the interested reader is referred to [6, 7, 14] and [8] for details.

The solver is based on a finite volume formulation with conservative variables co-located at cell centred. The spatial discretization of the convective terms is done with second order ENO-type scheme. The diffusive terms are discretized with second order centred scheme. The time integration is done by second order implicit scheme (three points backward); the solution at each time step is done by pseudo-time integration by means of Euler implicit scheme with approximate factorization with local pseudo time step and multi-grid acceleration. The turbulent viscosity has been calculated by means of the one–equation model of Spalart and Allmaras [9]. Free surface effects are taken into account by a single phase level-set algorithm [6]. Complex geometries and multiple bodies in relative motion are handled by a dynamical overlapping grid approach [7]. High performance computing is achieved by an efficient shared and distributed memory parallelization [8].

3 PROPELLER MODEL

In CFD applications of marine hydrodynamics, the propeller is often modeled instead to be directly resolved: in fact, the characteristic time and spatial scales required to solve accurately propeller blade hydrodynamics differ up to two order of magnitude with respect to those characterizing the hull. Usually, the presence of the propeller is described by the "body force" approach: axial and tangential momentum sources are added to the Navier Stokes equations and distributed in a toroidal disk of finite thickness representing the propeller. Body forces are usually determined by actuator disk theories that assume axial-symmetric inflow conditions and optimal distribution of circulation, and therefore may provide an incomplete description of the propeller operating in maneuvering conditions, which is characterized by strong oblique flow effects. In this work, the same propeller model described in [1] has been further improved in order to account more accurately of the propeller loading (crucial for the correct estimation of rudder propeller interaction); in the following, the key points of the model are summarized:

- The axial and circumferential body forces follow the radial distribution suggested by Hough and Ordway [10]. In order to simulate the propeller dynamic behavior during a maneuver, the thrust and torque coefficients (i.e. K_T and K_Q) are not prescribed; instead, they are interactively evaluated from the real propeller open water curves. In particular, at each time step the propeller advance coefficient is evaluated by averaging the effective wake in correspondence of the first plane of the disk, and consequently:

$$J_{eff} = \frac{\iint \vec{V}(r,\theta) \cdot \vec{n} \; dr \; d\theta}{ND} \tag{1}$$

  where $\vec{V}(r,\theta)$ is the local velocity, $\vec{n}$ the normal to the propeller disk, N is propeller rate of revolution and D is the diameter. J_{eff} represent an effective advance coefficient, and, in order to be consistent with the propeller open water curves, should be properly corrected for the self-induction effect. To this aim, the longitudinal self-induction factor a (averaged) has been evaluated on the basis of the one–dimensional actuator disk theory, namely:

$$a = \sqrt{1 - 8\frac{K_T}{J^2\pi}} \tag{2}$$

  where K_T is the thrust coefficient and J is the advance coefficient. In order to match the strict relation between propeller load and self induction factor, a non linear equation should be solved at each time step; however, this is avoided for the sake of computational efficiency. In particular, at the end of each time step the actual advance coefficient is computed by means of the induction facto evaluated at the previous time step, i.e.:

$$J_{nom} = J_{eff}(1 - a_{n-1}) \tag{3}$$

It has to be noticed that the self–induction coefficient can be computed considering the propeller load distribution over infinitesimal circumferential sections, thus leading to a radially varying distribution of a or the complete actuator disk theory that accounts for the circumferential momentum imparted to the flow. However, as shown in 3, an average value is required in present application.

- In order to model the performance of the propeller functioning in oblique flow, the semi-empirical method of Ribner [11] has been followed for the evaluation of propeller in–plane force, defined as:

$$Y_P = k_s Z \frac{3}{4\pi} \frac{\partial C_L}{\partial \alpha} A_{side} \frac{F(a)}{1 + k_a \frac{3}{4\pi} \frac{\partial C_L}{\partial \alpha} A_{side}} \beta \tag{4}$$

with $F(a)$ the propeller load factor, defined as:

$$F(a) = \frac{(1+a)[(1+a) + (1+2a)^2]}{1 + (1+2a)^2} \tag{5}$$

being a the longitudinal induction factor, which should be evaluated at the actual time step. In the previous equations, β is the flow angle of attack in correspondence of the propeller disk, k_s and k_a are semi-empirical constant introduced for taking into account hub effects and non homogeneous distribution of the inflow over the propeller disk and A_{side} is the blade projected lateral area; Z is the number of propeller blades. In this case propeller force is the total in plane force, i.e. the resultant of the lateral and vertical components; the inflow angle is properly evaluated by averaging the velocity components of the fluid over the propeller disk.

In order to gain more insight into the effect of propulsion system to the response of the model, different simulations have been carried out: in particular, the effect of the lateral force and the self-induction velocity (i.e. underestimating the propeller loading) have been switched off (separately), and the resulting maneuvers compared to the one obtained with the complete propeller model.

4 GEOMETRY AND TEST CONDITIONS

A twin screw twin rudder tanker-like model is considered for the numerical simulations (figure 1); the model is fully appended with bilge keels, struts, A-brackets and shafts for two propellers) and a single rudder. The main non dimensional characteristics are reported in table 1. For this model an extensive free running test program has been carried out at the lake of Nemi[12, 13], and numerical results are compared with those experimental data in terms yaw-checking parameter (rudder-heading angle plot). The data are shown only in non-dimensional form because of restriction on diffusion. All the quantities in the following are non-dimensionalized by a reference length $L = L_{pp}$ and the

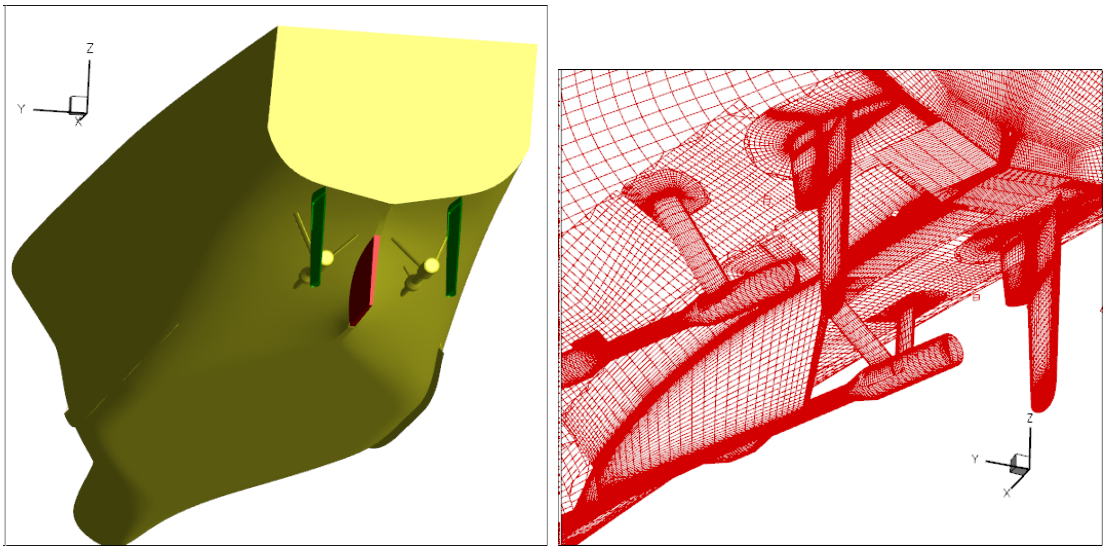

Figure 1: Left: model geometry overview. Right: mesh details around the stern region

approach velocity U_∞ (at model scale). This gives a Reynolds number $Re = 5.0 \times 10^6$ and a Froude number $F_N = 0.217$. Test cases considered are listed in 2; it has to be noticed that the effect of rudder angle rate of execution has been also investigated. The zig–zag tests are carried out at fixed turning rate of the propeller; the propulsion point is evaluated by means of a self–propulsion simulation.

Table 1: Ship model characteristics

L_{pp}	1
Speed	1
Displacement	$5.0987\,10^{-3}$
J	0.865
$Arud$	0.0023

5 COMPUTATIONAL MESH

The physical domain is discretized by means of structured blocks with partial overlap; overlapping grids capabilities are exploited to attain a high quality mesh and for refinement purposes. The whole mesh consists of a total of about 7.8 million of computational volumes. A detail of the discretization of the individual part of the vessel is summarized in table 3. Grid distribution is such that the thickness of the first cell on the wall is always below 1 in terms of wall units (y+=O(1) i.e. $\Delta/L_{pp} = O(20/Re)$, Δ being the thickness of the cell). In figure 1 detailed view of the mesh in the stern region is shown; the use of

Table 2: Test Matrix

TEST	$\dot{\delta}$ [deg/s]	Lateral Force	a
NUM.1	15	yes	yes
NUM.2	7.5	yes	yes
NUM.3	15	yes	no
NUM.4	15	no	yes

overlapping grid capability allowed to take into account for all the details, in particular for the mesh around the rudder where both the fixed and the mobile parts are carefully discretized.

Table 3: Test Matrix

Zone	N. of Blocks	N. of Cells
Background	2	184,320
Free surface	2	933,888
Hull	18	2,738,176
Bilge keels	8	655,360
Shafts and struts	24	733,184
Rudder	68	2,195,456
Skeg	34	299,008
Actuator disk	2	65,536

In the present work numerical computations have been carried out only on the medium mesh level, the activity on the finest mesh is still in progress.

6 RESULTS

In this paragraph numerical results for the cases listed in table 2 are discussed and compared with respect to the free running experiments. In table 4 the series of experimental data available are summarized in terms of the first and second overshoot angles and the equivalent overshoot times. The average value of the first and second overshoot angles are close to 8° and 9°, respectively; moreover, despite the relatively low number of experimental tests, the quantitative information of the measurement can be considered reliable, considering that the free running tests were carried out in an outdoor basin,

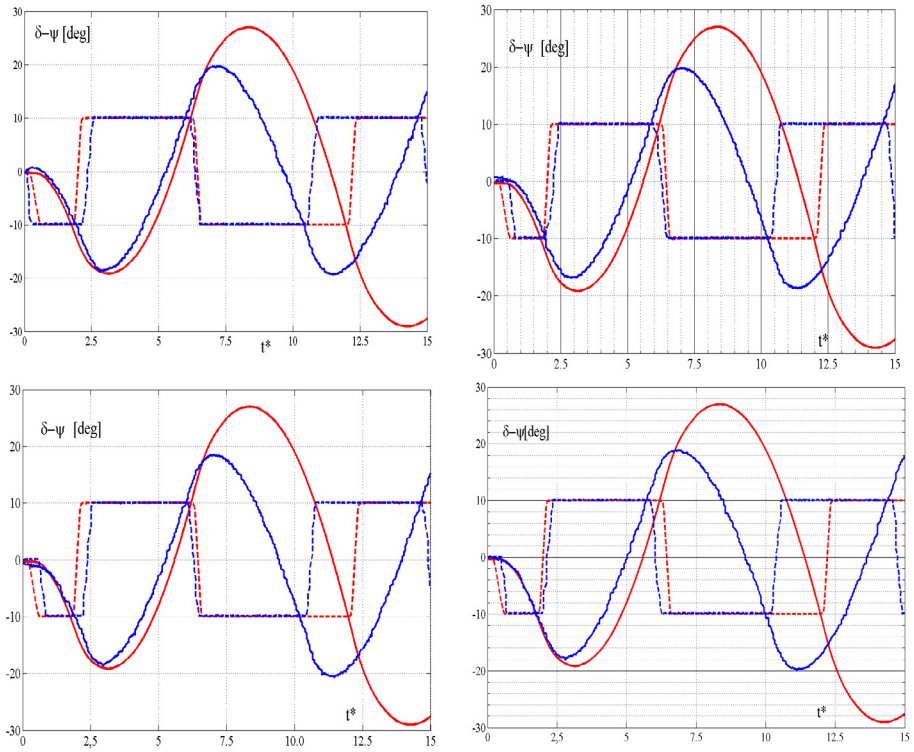

Figure 2: Comparison between simulated (–) and free running model tests (–)

and therefore some level of disturbance caused by wind can be expected. In table 4 yaw–checking parameters are reported.

Only the simulated maneuver with the complete propeller model (NUM.1) is compared with the experimental tests; the effect of propulsion and rudder rate is evaluated by comparing simulated maneuvers only. In the following discussion, the time is scaled by the characteristic time (i.e., $t^* = t\frac{U_\infty}{L_{pp}}$). In figure 2 the simulated maneuver is compared with all the free running tests available; the response of the vessel to the first rudder angle is in good agreement with measurements as well as the first overshoot angle. In the second part of the maneuver the discrepancy is noticeably higher: during the transient phase after the first counter-execution of the rudder (approximately at unit time $t = 2.5$), the yaw rate is higher and the vessel is less reactive to the rudder inversion at the second "yaw reach" (at time unit $t = 7$), leading to an excessive overshoot angle. It has to be noticed that the overestimation of the yaw rate could have been affected by discrepancies among the rotational mass of gyration, presently estimated by the equivalent ellypsoid method, i.e. $I_{zz} = \rho_\Delta \Delta$, where Δ is the model displacement and ρ_Δ represents the radius of gyration set equal to $0.25 L_{pp}$). Moreover, unsteady effects mainly related to propeller added mass, actually not included in the actuator disk model, may play a relevant role on the dynamic response of the vessel.

Table 4: Experimental results

TEST	$1^{st}ov$ [deg]	T_{1ov}	$2^{st}ov$ [deg]	T_{2ov}
EXP.1	8.51	1.12	9.65	1.29
EXP.2	6.79	1.06	9.73	1.17
EXP.3	8.68	1.12	8.41	1.05
EXP.4	8.17	1.06	8.74	1.17

Table 5: Numerical results

TEST	$1^{st}ov$ [deg]	T_{1ov}	$2^{st}ov$ [deg]	T_{2ov}
NUM.1	9.13	1.45	16.98	2.13
NUM.2	14.05	1.77	24.5	1.77
NUM.3	9.02	1.33	17.36	2.24
NUM.4	9.02	1.33	16.22	1.96

The propulsion system does not provide any remarkable effect on the model maneuvering response (see table 5 and figure 3); this is supported by comparison of simulation $NUM.1$ (red line) with $NUM.3$ (light blue line) and $NUM.4$, respectively. It can be evidenced that in the first transient phase (up to the 1^{st} overshoot angle) the vessel response very similar in all three cases. Discrepancies are more evidenced approaching the second overshoot phase: without the propeller lateral force the model experiences a slight improvement in yaw checking ability, with an overshoot angle lower than 2° with respect to $NUM.1$ and $NUM.4$, i.e., the propeller effect is destabilizing. As deeply discussed in [3], this effect has to be mainly addressed to a strong blockage of the rudders (which are located behind propellers) that causes a (lateral) up–wash in correspondence of the propeller plane. On the other hand, propeller loading slightly reduces the yaw checking ability of the vessel (the 2^{nd} overshoot angle is higher than in case of $NUM.1$): this effect is mainly related to propeller–rudder interaction, namely the decrease of propellers slipstream velocity affects rudder lift efficiency. Finally, it has to be emphasized that the rudder rate strongly affects the model response; this is evidenced since the 1^{st} overshoot angle and is dramatic in the second phase of the maneuver (2^{nd} overshoot angle close do 25°).

In order to gain further insight into the behavior of the rudder–propeller system during an unsteady maneuver, in figures 4-6 propeller forces in terms of thrust and lateral force ratio (i.e., $\frac{K_Y}{K_T}$, where K_Y represents the propeller lateral force coefficient) and rudder lateral force have been investigated for the reference maneuver $NUM.1$ and the most unstable one $NUM.2$. As evidenced in the plots, vertical lines are drawn for identifying the

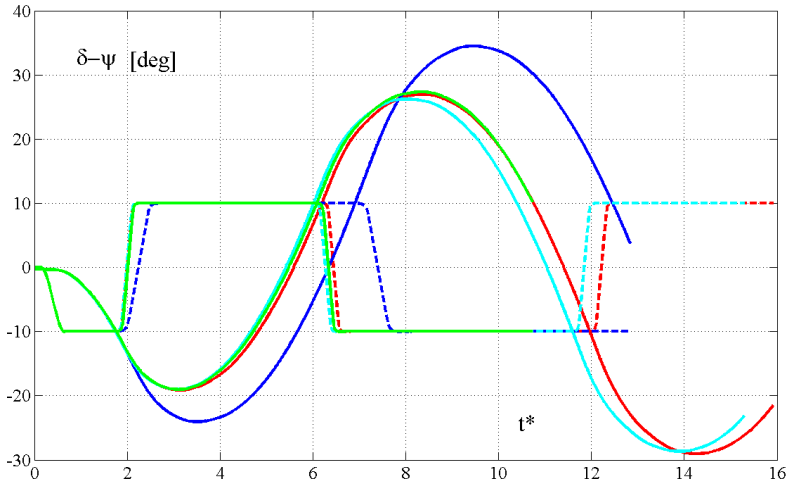

Figure 3: Simulation results; (–)$NUM.1$;(–)$NUM.2$;(–)$NUM.3$;(–)$NUM.4$

time instants relative to "yaw reach" (i.e. $\delta = \psi$, green lines) and to the heading overshoot (dark lines). The thrust coefficient (figure 4) for the $STBD$ and $PORT$ propellers shows a similar trend in both maneuvers; after the first rudder execution, the thrust exerted by the two propellers reduces.

Across the overshoot phase ($2 < t^* < 3$) the $STBD$ propeller is more loaded than the $PORT$ one; in fact, during this phase, this propeller changes the position with respect to the instantaneous center of rotation, i.e. it is in a leeward side as the maneuver starts and is on the windward side before reaching the 1^{st} overshoot; vice-versa, the $PORT$ propeller changes its relative position from the wind to the lee side, probably when it starts to decrease around $t^* = 2.5$. Moreover, immediately after the overshoot, the thrust on the windward propeller ($STBD$ side) decreases, whereas the thrust increases on the leeward propeller until $t^* = 4$. Thereafter, the loads on the two propellers experience a similar value and decrease up to the second "yaw reach". It has to be emphasized that the thrust variation around the overshoot is related to transient variations of the propeller inflow (mainly due to the change of the yaw rate and rudder blockage) that stabilize when a quite constant yaw rate is established ($4 < t^* < 6.5$). This phenomenon is different for the lee and windward propeller, because of the different flow straightening coefficient of the hull on the internal and external sides [2, 3]. This phenomenon is repeated during the second overshoot phase ($7.5 < t^* < 9$), with higher values of thrust because in this phase the model drift is relatively larger than before. Highest peaks are evidenced in case of $NUM.2$, because the model experiences a large drift and, consequently, a greater speed drop with respect to $NUM.1$. The propellers exert side–forces with opposite sign (see figure 5), and consequently, a negligible contribution to the dynamic response of the vessel is provided; it is worth of note the peaks in correspondence of the two "yaw checking" points ($t^* = 2$ and $t^* = 6.5$), probably caused by the rudder angle inversion which changes

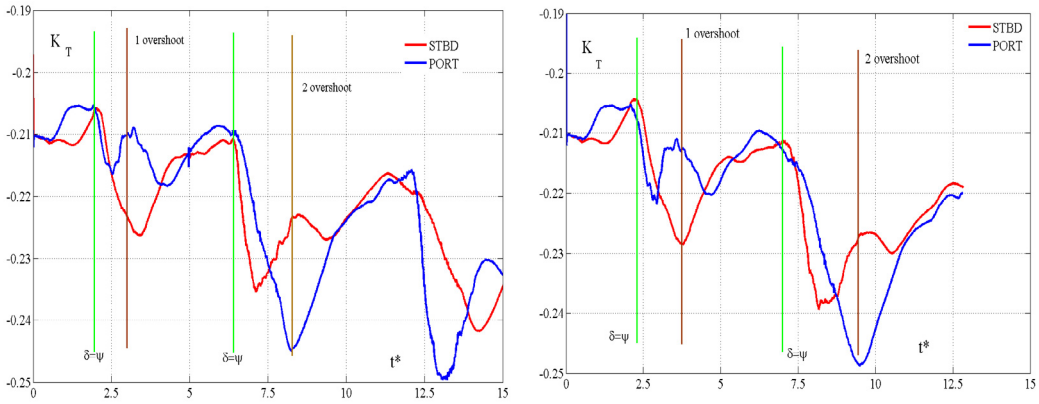

Figure 4: Thrust variation on the STBD and PORT propellers. Left: $NUM.1$ Right: $NUM.4$

the inflow drift angle in correspondence of the propellers (see also figure 6). Moreover, the trends of lateral forces across the yaw speed inversion show a similar behavior of the thrust coefficient K_T. Simulation $NUM.2$ shows a similar trend, with slightly larger peaks, consistently with the previous discussion. As discussed previously, effects of these transient on the propeller behavior is not entirely captured by the quasi-steady approach at the basis of the adopted propeller model. For the sake of completeness, time variation of the $STBD$ and $PORT$ rudders lateral force is depicted in figure 6; in the approach phase, the rudder forces are oppositely directed due to the flow "closure" direction at the stern. Consequently to the first rudder execution, the incidence angle of the $STBD$ rudder increases, whereas the one on the $PORT$ rudder decreases approximately with same rate and the model response is not immediate; after this short transient the model starts to yaw, and the rudder incidence angle progressively reduces. At the first rudder inversion, on both sides the lateral force increases noticeably until reaching a peak ($t^* = 2.3$) and then reduces due to the vehicle response (for the same reason as before). It has to be emphasized that during some intervals, the lateral force exerted by the rudder is opposite, i.e. one of the rudder is working like a stabilizing fin. Moreover, in correspondence of the overshoot transient, both rudders experiences stall phenomena (evidenced by the high frequency oscillations); the $STBD$ rudder is not affected by stall after the first rudder inversion, because the amplitude of hull motion is relatively lower.

7 CONCLUSIONS

In this work a preliminary investigation of the yaw checking ability of a twin screw twin rudder vessel experiencing poor course stability qualities has been carried out by means of an high accurate CFD solver. Different simulations have been carried out in order to validate a simplified propeller generalized for capturing oblique flow effects and, at the same time, to analyze the propeller contribution on unsteady maneuvering response of this challenging hull model. As a result, propeller effect as well as propeller loading

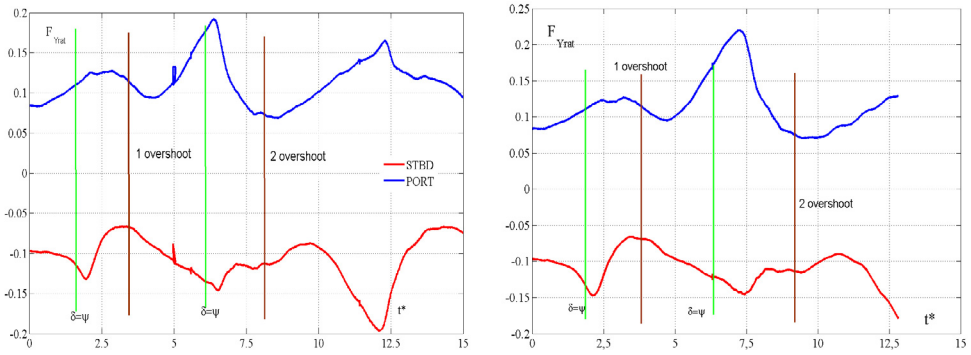

Figure 5: Lateral force coefficient on the STBD and PORT propellers. Left: $NUM.1$ Right: $NUM.2$

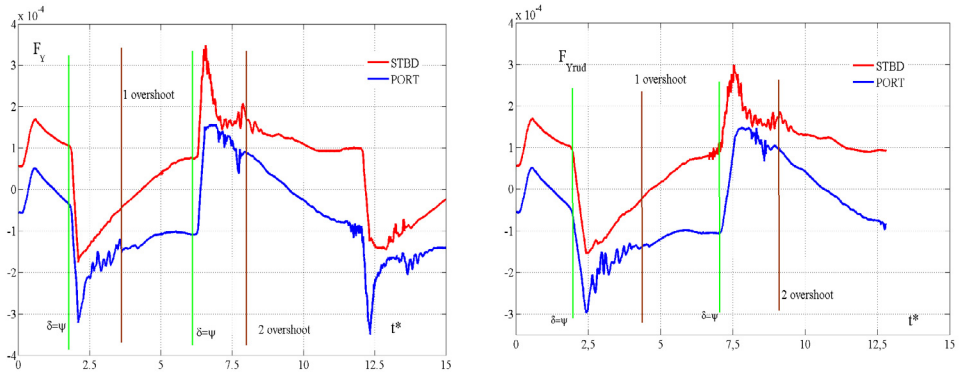

Figure 6: Lateral force on the STBD and PORT rudders. Left: $NUM.1$ Right: $NUM.2$

provide a negligible effect on this type of maneuver, because hull drift angle is low as well as the speed reduction. Comparison with free running experiments have been carried out in terms of yaw checking parameters; comparison is satisfactory in terms of first overshoot angle, whereas the second overshoot angle is over–predicted. Further work is required in order to investigate propeller effects that are still not included in the propeller model (i.e. added mass) and the vehicle behavior during tighter unsteady maneuver (i.e. zig-zag 20°-20°) and different stern appendage configuration (single rudder).

8 ACKNOWLEDGEMENTS

The authors are grateful to Dr. Salvatore Mauro for providing experimental data and for his useful suggestions and discussion on ship maneuvering related topics.

REFERENCES

[1] Broglia, R. and Dubbioso, G. and Durante, D. and Di Mascio, A. Simulation of Turning Circle by CFD: Analysis of different propeller models and their effect on

manoeuvring response *Applied Ocean research* (2013) **39**:1–10.

[2] Dubbioso, G., Durante, D., Broglia, R. and Di Mascio, A. CFD Manoeuvering Prediction of a Twin Screw Vessel with different stern appendages configuration 29^{th} *Symposium on Naval Hydrodynamics* (2012) Gothenburg, Sweden, 26–31 August.

[3] Broglia, R., Durante, D., Dubbioso, G. and Di Mascio, A. Turning ability characteristic study of a twin screw vessel by CFD *V Int. Conf. on Comp. Meth. in Marine Eng.* (2011), Lisbona

[4] Dubbioso, G. Maneuvering Behavior of Twin Screw Naval Vessels. *Phd Thesis* (2011) University of Genova, Italy.

[5] Amini, H. and Steen, S. Theoretical and experimental investigation of propeller shaft loads in transient conditions. *Int. Ship. Progress* (2012), **59**:55–82.

[6] Di Mascio, A. and Broglia, R. and Muscari, R. On the Applications of the One-Phase Level–Set Methods for Naval Hydrodynamic Flows *Computer and Fluids* (2007),**36(5)**:868–886.

[7] Di Mascio, A. and Muscari, R. and Broglia, R. An overlapping Grids Approach for the Moving Bodies Problems *Proc. of* 16^{th} *Offshore and Polar Engin. Conf.* (2006), San Francisco, California (USA).

[8] Broglia, R. and Di Mascio, A. and Amati, G. A Parallel Unsteady RANS Code for the Numerical Simulations of Free Surface Flows *Proc. of* 2^{nd} *International Conference on Marine Research and Trasportation* (2007), Ischia, Napoli (Italy).

[9] Spalart, P.R. and Allmaras, A. A One Equation Turbulence Model for Aerodynamic Flows *La Recherce Aerospatiale* (1994),**1**:5–21.

[10] Hough, G.R. and Ordway, D.E. The generalized actuator disk. *Development in Theorethic and Applied Mechanics* (1965), **2**:317–336.

[11] Ribner, H. Propellers in yaw. *NACA annual report* (1945),**31**:193–215.

[12] Mauro, S. (1999a). *Prove di Manovrabilità su Modello di Unità Logistica*. INSEAN Technical Report, N6/C 2280.

[13] Mauro, S. (1999b). *Prove di Manovrabilità su Modello di Unità Logistica*. INSEAN Technical Report, N8/C.2280.

[14] Di Mascio, A., Broglia, R., and Muscari, R. (2009). Prediction of hydrodynamic coefficients of ship hulls by high-order Godunov-type methods. *J. Marine Sci. Tech.*, 14:19–29.